

# Synthesis of Ag/NiO composite nanosheets and empty microspheres and their highly effective electrocatalytic properties

Lu Pan · Shanshan Ma · Li Li · Yonghong Chen

Received: 22 April 2014 / Accepted: 30 June 2014 / Published online: 8 July 2014  
© The Author(s) 2014. This article is published with open access at Springerlink.com

**Abstract** Ag/NiO composite nanosheets and empty microspheres were fabricated by calcining the precursors synthesized via hydrothermal and solvothermal procedures involved four methods. The as-prepared samples were characterized by thermogravimetric and differential thermal analysis, X-ray diffraction, X-ray photoelectron spectroscopy, transmission electron microscopy and field emission scanning electron microscopy, respectively. The electrocatalytic properties of Ag/NiO composites modified on a glassy carbon electrode for *p*-nitrophenol reduction were investigated. The results showed that Ag/NiO composites exhibited highly enhanced electrocatalytic activity than a bare glassy carbon electrode, for not only the peak current increased clearly but also the corresponding peak potential decreased markedly. As a comparison, two NiO samples were used and the results showed that the peak current has an increase but the peak potentials have a slight decrease by comparing to a bare glassy carbon electrode. The Ag/NiO composites have the potential application in the electrocatalysis for the reduction of nitrophenol materials.

**Keywords** Ag/NiO composites · Nanosheets · Empty microspheres · Electrocatalysis · *p*-Nitrophenol

## 1 Introduction

The significant transition metal oxides with nanostructures generally possess numerous highlighted physicochemical properties and have been applied widely in catalysts [1–4], electrochemistry [5, 6], gas sensors [7, 8], biomedical materials [9, 10] and other fields. Of the oxides, nickel oxide (NiO), an important *p*-typed semiconductor with stable band gap, has received much attention and been extensively studied and used frequently as electrode for lithium ion batteries and fuel cells [11, 12], catalysts [13–15], electrochemical supercapacitors [16, 17], dye-sensitized photocathodes [18], magnetic materials [19, 20], etc. However, with fast advancements in all areas of industry and technology, the pure NiO nanomaterials do not meet with the increasingly expanding demands. To effectively expand the performances and broaden the applications of NiO, the focus on the investigation of nickel oxide mixing or doping with metals or other transition metal oxides have attracted much attention in recent decades, because the mixing or doping of other metals or transition metal oxides with nickel oxide can produce new composite materials which may exhibit more novel physical and chemical properties [21–26]. Noble metals with a great deal of excellent properties are mingled or doped in NiO [27–30]. Of the noble metals, silver with the lowest price and good properties has been utilized most frequently. In the previous reports, Ag/NiO micro and nanomaterials have shown outstanding electrical conductivity [31], catalytic performances for CO oxidation [32], photocatalytic property [33], sensor [34], and so on. However, the electrocatalytic property of Ag/NiO composite modified on a glassy carbon electrode (GCE) has been involved seldom. In the work, Ag/NiO composite nanosheets and empty microspheres were prepared

L. Pan (✉) · S. Ma · L. Li · Y. Chen  
Department of Chemistry and Chemical Engineering, Huainan Normal University, Huainan 232001, China  
e-mail: panlu1970@163.com

L. Pan · Y. Chen  
Anhui Key Laboratory of Low temperature Co-Fired Material, Huainan Normal University, Huainan 232001, China

respectively by using four methods. The Ag/NiO samples were modified on a GCE, and their electrocatalytic performances for *p*-nitrophenol reduction in a base solution were investigated in detail. The experiments demonstrated that the modified GCEs showed high electrocatalytic activity.

## 2 Experimental

### 2.1 Chemicals

AgNO<sub>3</sub>, Ni(NO<sub>3</sub>)<sub>2</sub>·6H<sub>2</sub>O, N(CH<sub>2</sub>CH<sub>3</sub>)<sub>3</sub>, (CH<sub>2</sub>)<sub>6</sub>N<sub>4</sub>, urea, sodium tartrate, polyvinylpyrrolidone (PVP K-30), polyethylene glycol (PEG 6000), sodium dodecyl sulfate (SDS), and ethanol were purchased from Shanghai Reagent Co., China. All chemicals were used without any further treatment as received.

### 2.2 Sample synthesis

*Synthesis of Ag/NiO nanosheets* Ag/NiO nanosheets could be prepared with two methods. Method 1 could be described as the following: AgNO<sub>3</sub> and Ni(NO<sub>3</sub>)<sub>2</sub>·6H<sub>2</sub>O with total 2.5 mmol and 0.5 g PVP were dissolved completely under rigorous magnetic agitation in 45 mL of distilled water in 100 mL of beaker, then 10 mmol of (CH<sub>2</sub>)<sub>6</sub>N<sub>4</sub> was added into the above system, finally the mixture was transferred into 60 mL of Teflon-lined stainless steel autoclave, which was sealed and maintained at 140 °C for 12 h. When the autoclave was cooled to room temperature naturally, and the precursor was filtered and washed with distilled water then ethanol for several times, and dried in vacuum at 80 °C for 12 h. By the calcination of the dried precursor at 400 °C for 3 h, the sheet-like Ag/NiO samples with different Ag contents were prepared. Ag/NiO nanosheets also could be fabricated in method 2. AgNO<sub>3</sub> and Ni(NO<sub>3</sub>)<sub>2</sub>·6H<sub>2</sub>O with total 2.5 mmol and 0.5 g PEG were dissolved completely under rigorous magnetic agitation in 45 mL of distilled water in 100 mL of beaker, then 2.5 mL of N(C<sub>2</sub>H<sub>5</sub>)<sub>3</sub> was added into the above system by dropwise and the stirring was kept for 30 min, finally the mixture was transferred into 60 mL of Teflon-lined stainless steel autoclave. The followed preparation procedures were the same with the ones used in method 1.

*Synthesis of Ag/NiO empty microspheres* Synthesis of Ag/NiO empty microspheres also could be synthesized used two methods. In method 3, the precursor of Ag/NiO empty microspheres was prepared via a solvothermal procedure referred to the previous report after a bit alteration [35]. In a typical synthesis, AgNO<sub>3</sub> and Ni(NO<sub>3</sub>)<sub>2</sub>·6H<sub>2</sub>O with total 2.5 mmol were dissolved fully in a solvent composed of 30 mL of absolute ethanol and 15 mL of

distilled water, then 0.15 g of SDS and 20 mmol of urea were added to the above solution, subsequently the mixture was transferred into 60 mL of Teflon-lined stainless steel autoclave, which was sealed and maintained at 110 °C for 15 h. As the autoclave was cooled naturally to room temperature, the precursor was filtered and washed with distilled water then ethanol for several times, and dried in vacuum at 80 °C for 10 h. By the calcination of the dried precursor at 400 °C for 3 h, the empty sphere-like Ag/NiO samples with different Ag contents were prepared. In method 4, the precursor of Ag/NiO empty microspheres was prepared via a hydrothermal method. Typically, AgNO<sub>3</sub> and Ni(NO<sub>3</sub>)<sub>2</sub>·6H<sub>2</sub>O with total 2.5 mmol, and 1 g of PEG, and 20 mmol of urea, and 5 mmol of sodium tartrate were dissolved completely in 45 mL of distilled water, and a homogeneous solution was obtained. The mixture was transferred into 60 mL of Teflon-lined stainless steel autoclave. The autoclave was maintained at 180 °C for 18 h. The subsequent steps were same with the ones used in method 3.

The detailed synthesis parameters and corresponding products are listed in Table 1.

### 2.3 Characterization

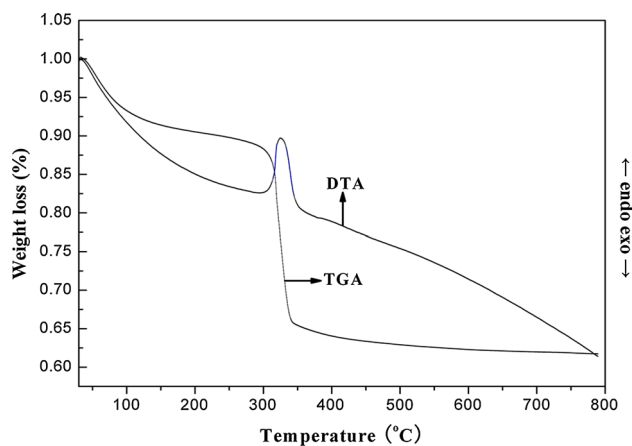
Thermogravimetric and differential thermal analysis experiments were performed on a Shimadzu TA-50WS analyzer in N<sub>2</sub> gas in the temperature range from room temperature to 780 °C. The phases testing of the final samples was examined by a Philips X'Pert PROSUPER X-ray diffraction (XRD) with Cu K $\alpha$  radiation ( $\lambda = 0.154178$  nm), using an operation voltage and current of 40 kV and 50 mA. X-ray photoelectron spectroscopic (XPS) measurement was performed with an ESCALAB 250 VG Lited XPS operated at 15 kV ( $h\nu = 1,486.6$  eV). The TEM images were collected on a Hitachi Model H-800 transmission electron microscopy, using an accelerating voltage of 200 kV. The FE-SEM images were carried on a JEOL-6300F FE-SEM with accelerating voltage of 15 kV.

### 2.4 Electrochemical determination

The electrocatalytic measurements were carried out on LK 98 microcomputer-based electrochemical system (Tianjin Lanlike Chemical and Electron High Technology Co., Ltd., Tianjin in China). A three-electrode single compartment cell was used for cyclic voltammetry. A GCE (3.7 mm in diameter) was used as working electrode and a platinum plate (Pt) as counter electrode and a Ag/AgCl electrode as reference electrode. Before determination, the surface of a GCE was polished carefully on an abrasive paper first, further polished with 0.3 and 0.05  $\mu\text{m}$   $\alpha$ -Al<sub>2</sub>O<sub>3</sub> paste in turn, and then rinsed completely with doubly distilled water

**Table 1** Synthetic condition of Ag/NiO samples in different projects and their resulting morphologies

Method	Chemicals	Preparation method	Reaction condition	Morphology of samples
1	AgNO <sub>3</sub> + Ni(NO <sub>3</sub> ) <sub>2</sub> + (CH <sub>2</sub> ) <sub>6</sub> N <sub>4</sub> + PVP	Hydrothermal	140 °C for 12 h	Nanosheets
2	AgNO <sub>3</sub> + Ni(NO <sub>3</sub> ) <sub>2</sub> + N(C <sub>2</sub> H <sub>5</sub> ) <sub>3</sub> + PEG	Hydrothermal	140 °C for 12 h	Nanosheets
3	AgNO <sub>3</sub> + Ni(NO <sub>3</sub> ) <sub>2</sub> + urea + SDS + C <sub>2</sub> H <sub>5</sub> OH	Solvothomal	110 °C for 15 h	Empty microspheres
4	AgNO <sub>3</sub> + Ni(NO <sub>3</sub> ) <sub>2</sub> + urea + tartrate + PEG	Hydrothermal	180 °C for 24 h	Empty microspheres

**Fig. 1** TGA–DTA curves of the precursor of NiO prepared in method 4

and absolute alcohol. A 20 mg of sample was dispersed in 4 mL of doubly distilled water under ultrasonication conditions to obtain a suspension solution. Of the suspension solution, 50  $\mu$ L was withdrawn and covered on the surface of carbon of the GCE. After dried automatically in air, a modified GCE was prepared and used directly for electrochemical measurement.

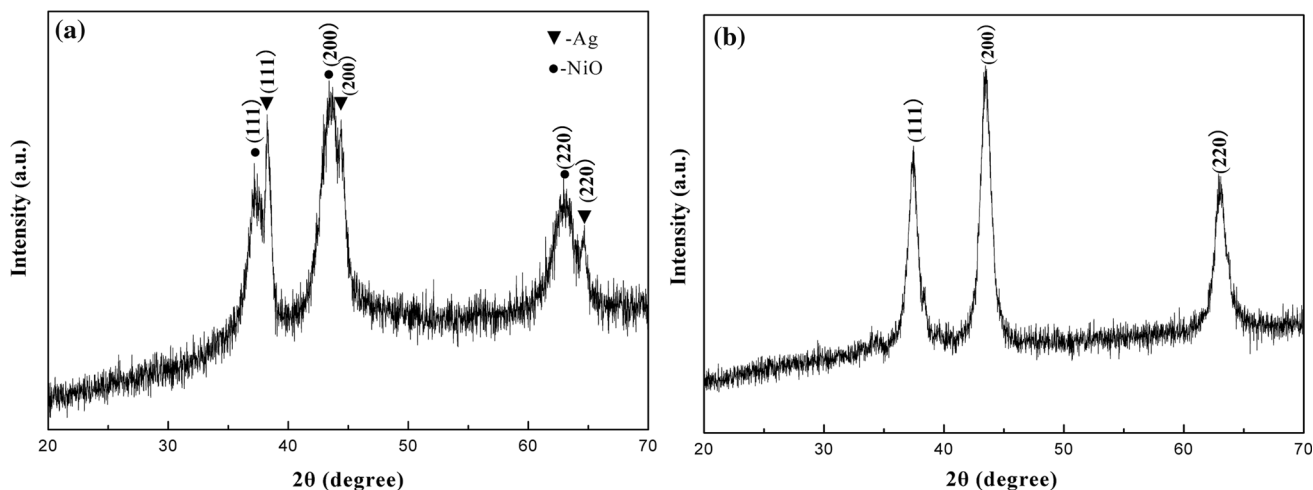
### 3 Results and discussion

To determine the decomposition temperature of the precursor, the thermogravimetric and differential thermal analysis experiments of the precursor without addition of Ag prepared in method 4 were carried out. The results are shown in Fig. 1. From the DTA curve, there is an endothermic peak locating at between 290 and 350 °C, which indicates that the precursor begin to decompose and form NiO at the interval temperatures. From the TGA curve, two weight losses are detected clearly locating at between room temperature to 120 and 290–350 °C, respectively. The first weight loss can be attributed to desorption of inorganic and organic molecules absorbed on the precursor, which is pertinent to the physical process and no endothermic peak

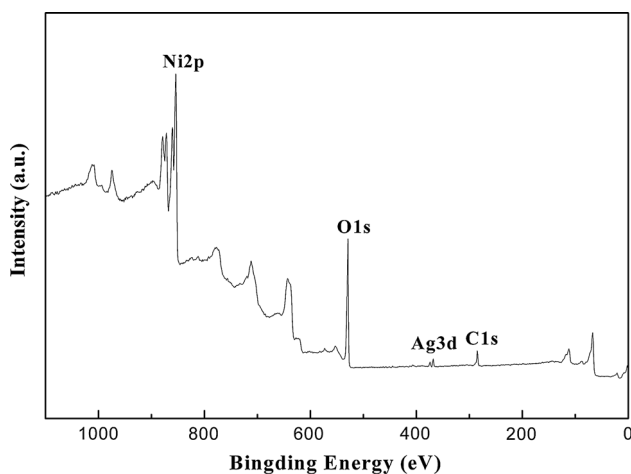
on the DTG curve can be detected. The second one is ascribed to decomposition of the precursor into NiO sample, which accompanies a strong chemical endothermic peak. By increasing temperature in the range from 350 to 780 °C, the weight loss does not occur, verifying formation of the stable NiO phase. Based on the TGA–DTA experiments, NiO sample can be fabricated by incinerating its precursor over 350 °C. In the work, the NiO in method 4 was synthesized by calcining its precursor at 400 °C for 3 h. The other experiments demonstrated that all the NiO samples in method 1–3 could be prepared by calcining the corresponding precursors at 400 °C for 3 h. For the precursor containing Ag, as temperature is over 200 °C, Ag phase is in stability. [36]. Hence, all the Ag/NiO composites were fabricated by calcination of each precursor at 400 °C for 3 h.

Figure 2 shows the XRD patterns of Ag/NiO samples with 5 % Ag content prepared in method 1 (Fig. 2a) and 2 (Fig. 2b), respectively. From Fig. 2a, the characteristic diffraction peaks are finely indexed as face-centered cubic NiO phase which corresponds to (111), (200) and (220) crystalline planes and a cubic Ag phase which is due to (111), (200) and (220) crystalline planes, respectively. No other diffraction peak is detected, which demonstrates that the as-synthesized composite is composed of Ag and NiO. The width of the diffraction peaks of both Ag and NiO broadens obviously, which is indicative of weak crystallization and small size of the sample. From Fig. 2b, however, only the characteristic diffraction peaks which are attributed to face-centered cubic NiO phase corresponded to (111), (200) and (220) crystalline planes are detected, and the predominantly characteristic diffraction peaks of Ag phase of (111), (200) and (220) planes, which stand at 38, 44 and 64 °C or so at  $2\theta$  values are not observed. The main reason may be explained as that a small amount of Ag nanoparticles with a small size are dispersed finely in the crystal lattices of NiO phase.

To verify the composition of the Ag/NiO with 5 % Ag prepared in method 2, the XPS experiment was carried out. The survey XPS spectrum of the sample is shown in Fig. 3. From Fig. 3, C1s peak locates at 284.6 eV, and except C,



**Fig. 2** XRD patterns of Ag/NiO with 5 % Ag prepared in method 1 (a) and in method 2 (b)



**Fig. 3** XPS spectrum of Ag/NiO with 5 % Ag content prepared in method 2

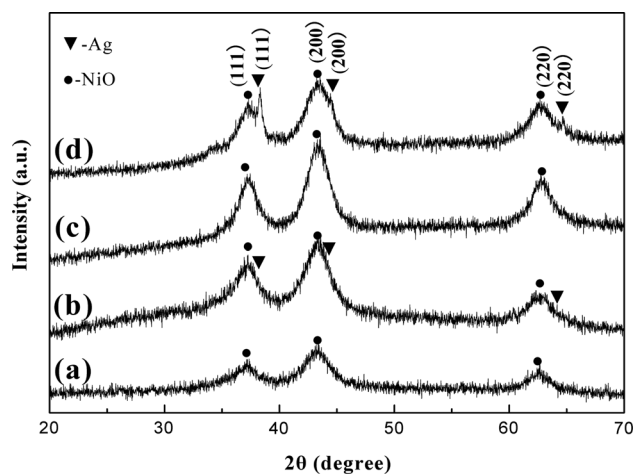


**Fig. 4** XRD patterns of NiO (a) and Ag/NiO with 3 % Ag (b) prepared in method 3, NiO (c) and Ag/NiO with 3 % Ag (d) prepared in method 4

Ag, Ni, and O, no peak due to other element can be detected, which indicates that the sample ought to be consisted of silver and nickel composite oxide. The calculated molar ratio of Ag and Ni is very close to the theoretical value. By combining the XRD pattern displayed in Fig. 2b and the XPS curve in Fig. 3, it can be confirmed the composition of the Ag/NiO composite.

Figure 4 shows the XRD patterns of NiO (a) and Ag/NiO with 3 % Ag (b) prepared in method 3 and NiO (c) and Ag/NiO with 3 % Ag (d) prepared in method 4, respectively. From curve a and c, all the characteristic diffraction peaks are in good agreement with the face-centered cubic NiO, no other peaks which are ascribed to Ni(OH)<sub>2</sub>, NiOOH or Ni<sub>2</sub>O<sub>3</sub> can be observed, indicating the formation of pure NiO. Additionally, the width of the peaks broadens obviously, which implies weak crystallization

and small size of the samples. According to curve b, however, all the diffraction peaks in the range from 20° to 70° in  $2\theta$  value of the Ag/NiO with 5 % Ag prepared in method 3 are mainly in well accordance with face-centered cubic NiO, and the characteristic diffraction peaks of cubic Ag phase are so weak that can be not observed clearly. Based on curve d, all the characteristic diffraction peaks which are attributed to both cubic phase Ag and face-centered cubic NiO are detected respectively, revealing the formation of composite Ag/NiO. Similarly, the width of the diffraction peaks in curve b and d becomes broad, also suggesting the weak crystallization and small size of the corresponding composites.

To verify the existence of Ag in the composite prepared in method 3, the XPS experiment of Ag/NiO with 3 % Ag

was performed. The result is exhibited in Fig. 5. From the survey XPS spectrum, except C (C1s peak locates at 284.6 eV), Ag, Ni, and O, there is no peak due to other element, which indicates that the composite may be composed of metal silver and nickel oxide. The determined molar ratio of Ag and Ni is very close to the theoretical value. Hence, it can be confirmed the composition of the Ag/NiO composite with 3 % Ag based on the curve b in Fig. 4 and the XPS curve in Fig. 5.

Figure 6 displays the TEM images of Ag/NiO with 5 % Ag (Fig. 6a) and 10 % Ag (Fig. 6b) prepared in method 1. From Fig. 6, the two composites exhibit sheet-like morphology. For the two samples, Ag nanoparticles with a

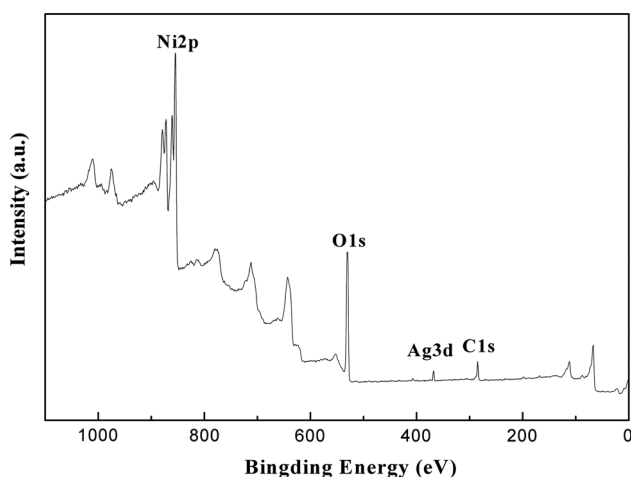


**Fig. 5** XPS spectrum of Ag/NiO with 5 % Ag content prepared in method 3

mean size of 10 nm or so are dispersed in NiO nanosheets, and Ag nanoparticles have a fine dispersivity. By increasing Ag amount from 5 % to 10, Ag nanoparticles in the composite increases obviously by comparing Fig. 6a, b. For the synthesis of Ag/NiO composite in method 1,  $(\text{CH}_2)_6\text{N}_4$  was added via a hydrothermal procedure. Ag nanoparticles could be produced easily via the reduction of  $\text{Ag}^+$  ions by HCHO released from the hydrolysis of  $(\text{CH}_2)_6\text{N}_4$  ( $(\text{CH}_2)_6\text{N}_4 + 6\text{H}_2\text{O} = 6\text{HCHO} + 4\text{NH}_3$ ) [37], and nickel ions hydrolyzed to form  $\text{Ni}(\text{OH})_2$ . Additionally, the addition of PVP could prevent Ag nanoparticles from agglomerating, leading to the formation of Ag nanoparticles with a mean size of 10 nm or so.

Figure 7 displays the TEM images of NiO (Fig. 7a) and Ag/NiO with 3 % Ag (Fig. 7b), 5 % Ag (Fig. 7c) and 10 % Ag (Fig. 7d), respectively, prepared in method 2. From Fig. 7, it can be seen clearly that NiO and Ag/NiO samples all are sheet-like morphology, and there are numerous caves in the nanosheets, which suggests that the nanosheets consist of nanoparticles. Furthermore, there are a certain amount of hexagonal nanosheets with a mean length of 50–60 nm in them. Additionally, a few nanorings in NiO sample (Fig. 7a) can be detected, but the nanorings can not be observed nearly in the Ag/NiO composites (Fig. 7b–d), which indicates that addition of Ag can affect the growth of NiO nanorings. For synthesis of Ag/NiO composites in method 2,  $\text{N}(\text{C}_2\text{H}_5)_3$  was used as reagent to react with  $\text{Ag}^+$  and  $\text{Ni}^{2+}$ , leading to the  $\text{Ag}_2\text{O}$  and  $\text{Ni}(\text{OH})_2$ . Furthermore  $\text{Ag}_2\text{O}$  did not transfer into coordination compound owing to the weak coordinating ability and alkalinity of  $\text{N}(\text{C}_2\text{H}_5)_3$ . Via a hydrothermal treatment,  $\text{Ag}_2\text{O}$  could be decomposed to Ag nanoparticles with a small size due to

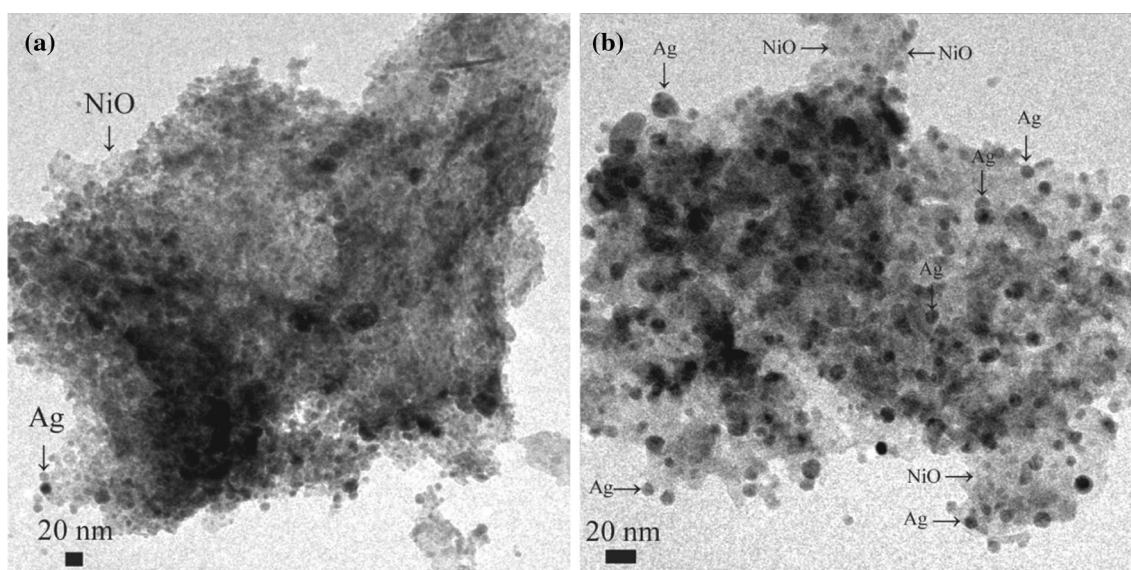


**Fig. 6** TEM images of Ag/NiO samples with 5 % Ag (a) and 10 % Ag (b) prepared in method 1

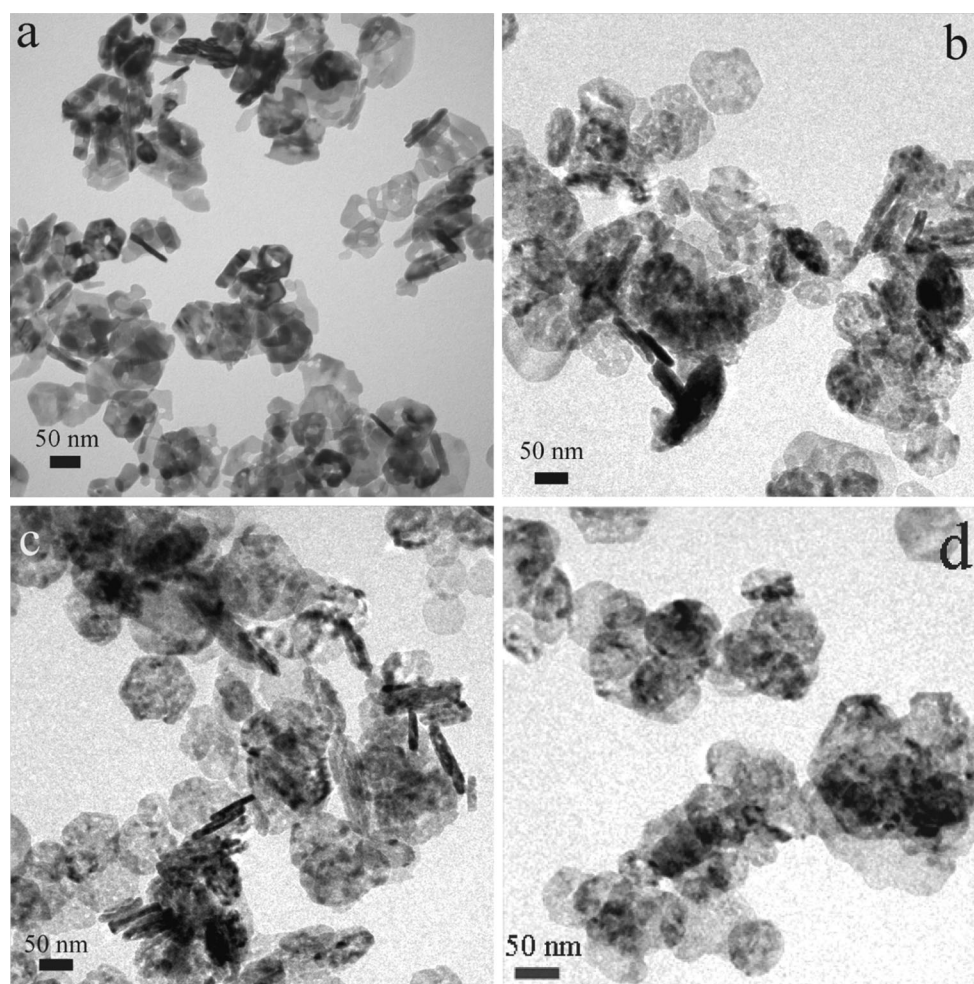


**Fig. 7** TEM images of Ag/NiO samples with 0 % Ag (a), 3 % (b), 5 % (c) and 10 % (d) prepared in method 2

the protection of PEG, and  $\text{Ni}(\text{OH})_2$  could grow into sheet-like morphology at 140 °C for 12 h. By calcining the corresponding precursor, the Ag/NiO nanosheets with hexagonal shape could be fabricated.

Figure 8 shows the TEM and FE-SEM images of NiO and Ag/NiO composites with different Ag contents prepared in method 3. From Fig. 8a, b, NiO is non-uniform sized empty microspheres assembled actually of numerous nanoplates with a mean thickness of 10 nm or so. The size of the larger microspheres reaches around 3  $\mu\text{m}$ . With addition of 1 % Ag, the Ag/NiO composite still possesses the empty sphere structure, and these microspheres also are composed of nanoplates (Fig. 8c–e). From the TEM images shown in Fig. 8c, d, the portion in center is blacker than the ones in border, which indicates the sample possesses empty structure. Based on Fig. 8f–h, similarly, the Ag/NiO composite with 3 % Ag still displays an empty microsphere structure. However, from the magnified FE-SEM image shown in Fig. 8h, the Ag/NiO composite is not assembled by nanoplates like the NiO or Ag/NiO with 1 %

Ag but by the worm-like structures which are composed possibly of nanoparticles. The change of the structure may be caused by the addition of a large amount of Ag. In the synthesis of method 3, SDS was used as surfactant which can serve as template, ethanol was used for solvent and the reductant of  $\text{Ag}^+$ , and urea hydrolyzed and decomposed into  $\text{NH}_3$  and  $\text{CO}_2$ .  $\text{NH}_3$  hydrolyzed with water and released hydroxyl anions which reacted with  $\text{Ni}^{2+}$  ions to form  $\text{Ni}(\text{OH})_2$  precursor. Meanwhile,  $\text{CO}_2$  could form numerous gaseous bubbles that served as heterogeneous nucleation centers for multi-crystalline aggregation, leading to formation hollow structured precursors. By incinerating the precursor, NiO and Ag/NiO empty microspheres could be prepared.

Figure 9 exhibits TEM and FE-SEM images of the Ag/NiO with 1 % Ag (Fig. 9a–c) and 3 % Ag (Fig. 9d, e) prepared in method 4. From Fig. 9, the Ag/NiO samples with different Ag contents all are the empty microspheres, and these microspheres have a uniform size of 380–400 nm. From Fig. 9c, the microspheres have a rather

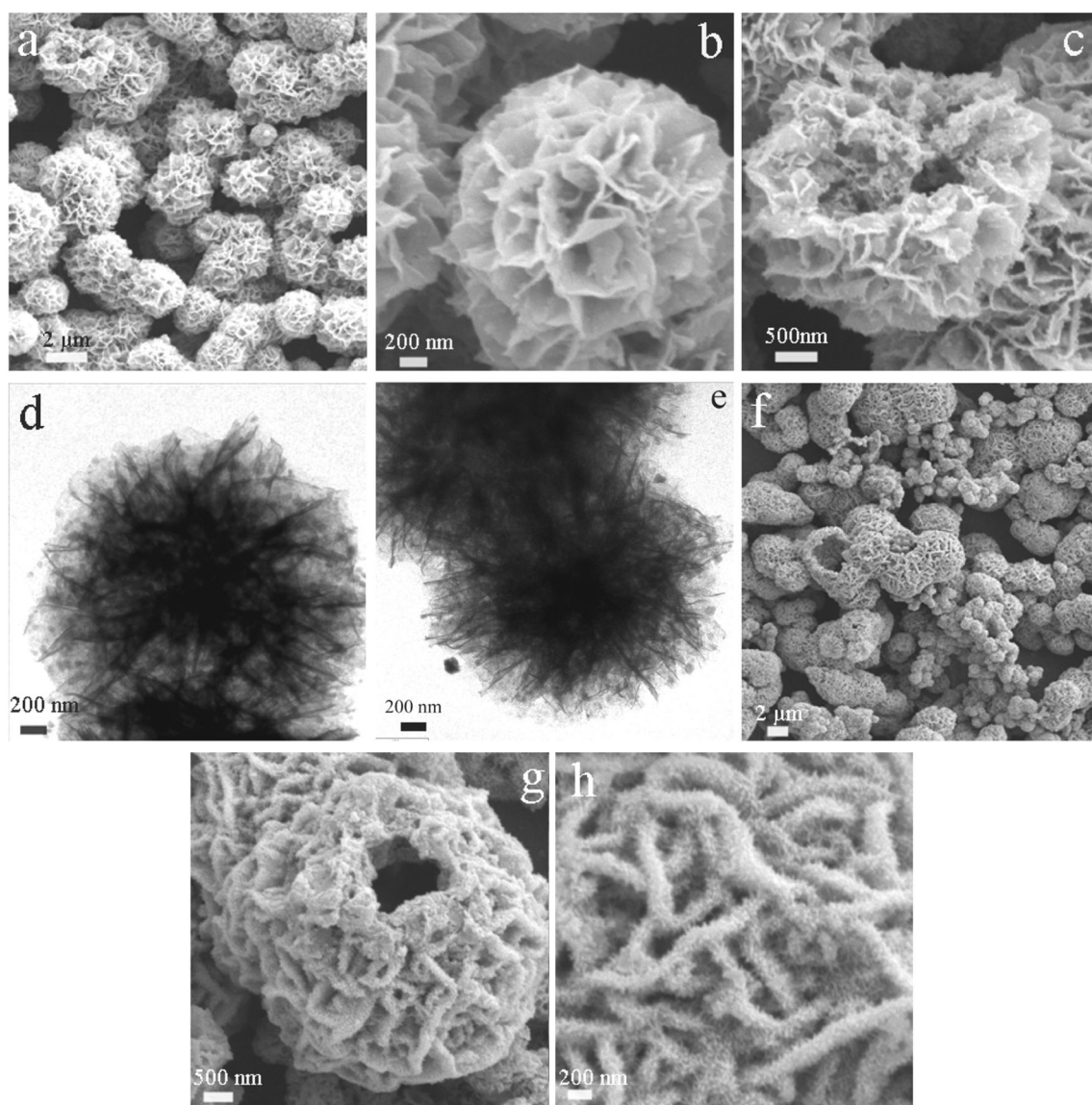


**Fig. 8** FE-SEM images of NiO (**a**, **b**), Ag/NiO with 1 % Ag (**c**), 3 % Ag (**f**–**h**), TEM images of Ag/NiO with 1 % Ag (**d**, **e**). The NiO and Ag/NiO samples prepared in method 3

high output. According to the TEM images, Ag nanoparticles with a mean size of 15 nm or so can be seen clearly, and these Ag nanoparticles are inset in the NiO empty microspheres which assembled by numerous NiO nanoplates with a mean size of 10 nm or so. By comparison with the samples prepared in method 3 and 4, the microspheres fabricated in method 4 not only have the smaller size but a rather uniform size than that in method 3. Although the growing mechanism of the samples prepared in method 4 is similar basically to the one in method 3, there is evident difference between them. The added sodium tartrate acted as ligand to  $\text{Ni}^{2+}$  and  $\text{Ag}^+$  ions, which could decrease effectively the free  $\text{Ni}^{2+}$  and  $\text{Ag}^+$  concentration and not only was favorable for the precursor

to grow orderly but restricted the precursor to grow fast. Hence, the final samples prepared in method 4 have a smaller size than the ones in method 3.

The electrocatalytic performances of NiO samples prepared in method 2 and 3 as well as Ag/NiO with 5 % Ag prepared in each method modified on a GCE for the reduction of *p*-nitrophenol in a base solution were investigated using a cyclic voltammetry method. The results are shown in Figs. 10 and 11. From Fig. 10, a bare GCE exhibits weak activity, for its peak current is only 40  $\mu\text{A}$  at a potential of  $-1.046$  V (curve 1). As the GCE modified with NiO prepared in method 2 and Ag/NiO with 5 % Ag prepared in method 1 and 2, respectively, the corresponding peak currents are 75, 89 and 86  $\mu\text{A}$ , respectively, which

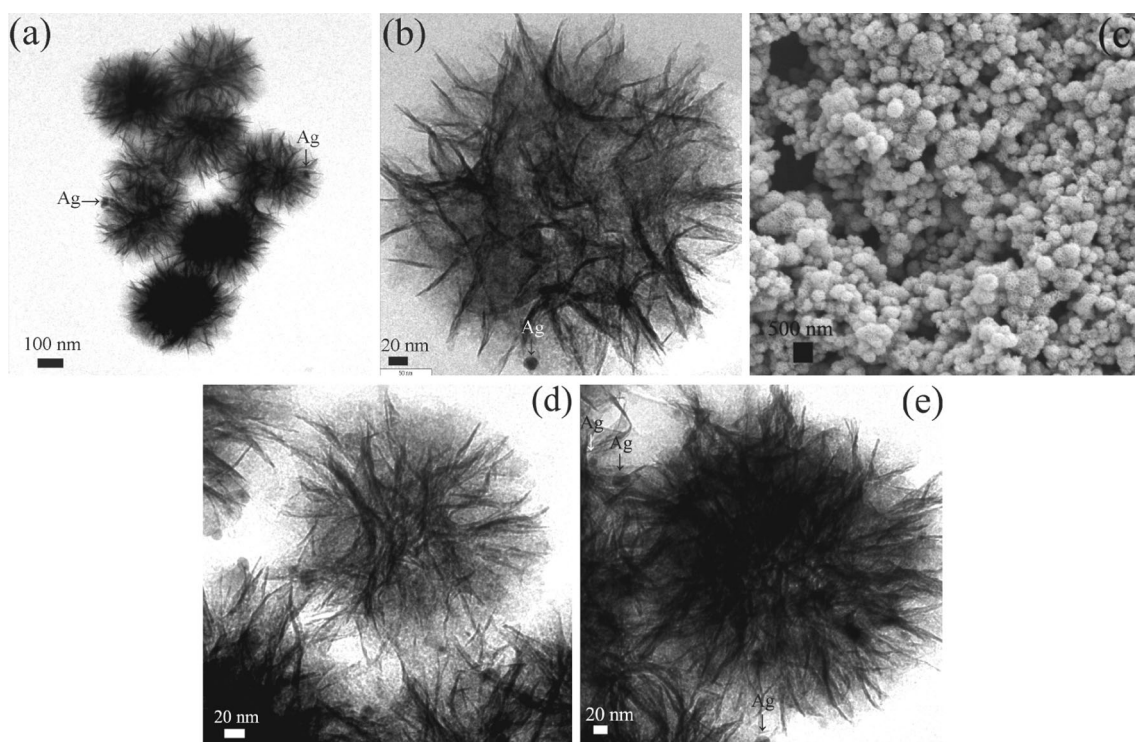


**Fig. 9** TEM images of Ag/NiO with 1 %Ag (a, b) and with 3 %Ag (d, e), FE-SEM image of Ag/NiO with 1 %Ag (c), the Ag/NiO samples prepared in method 4

potentials locate at  $-1.023$  (curve 2),  $-0.725$  (curve 3) and  $-0.739$  (curve 4), respectively. By comparison with a bare GCE, the modified GCEs all show an enhanced electrocatalytic activity, for the peak currents with NiO and Ag/NiO in method 1 and 2 are 1.9, 2.2 and 2.1 times bigger than that with a bare GCE. By comparing with the bare GCE, in spite of the increased peak current with NiO, its peak potential has a slight decrease with 0.023 V, however, the peak potentials have an obvious decrease with 0.321 and 0.307 V respectively by using the GCE with Ag/NiO with 5 % Ag prepared in method 1 and 2. From Fig. 11, by comparison with a bare GCE (curve 1), the GCE with NiO (curve 2) and Ag/NiO with 5 % Ag prepared in method 3 (curve 3) and Ag/NiO with 5 % Ag prepared in method 4 (curve 5) all display enhanced electrocatalytic activity, for the corresponding peak currents are 74, 82, 84  $\mu\text{A}$ , respectively at the potentials of  $-1.020$ ,  $-0.764$  and  $0.719$  V, respectively, and their peak currents are 1.9, 2.2 and 2.1 times bigger than that with a bare GCE. Similarly, by comparing to a bare GCE, although the peak current has an obvious increase with NiO, the peak potential has a slight decrease with 0.026 V. The Ag/NiO samples display effective electrocatalytic activity, for not only their peak currents have clear increase but also their peak potential decrease evidently with 0.284 and 0.327 V with the Ag/NiO in method 3 and 4, respectively. Based on Figs. 10 and

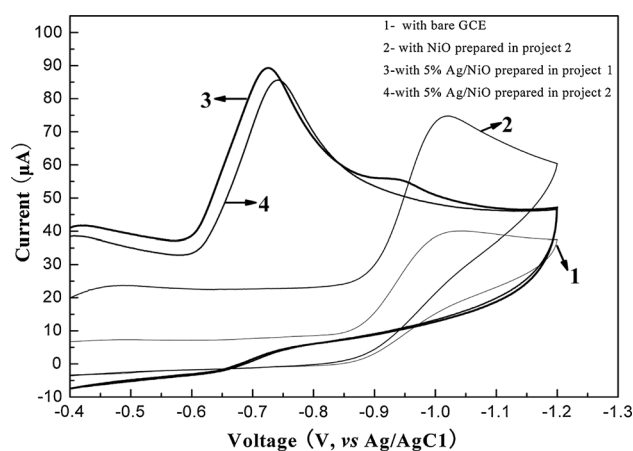


**Fig. 10** Cyclic voltammograms of a bare GCE (curve 1) and a GCE modified with NiO and Ag/NiO with 5 % Ag content prepared with addition of  $\text{N}(\text{C}_2\text{H}_5)_3$  (curve 2 and 4) and  $(\text{CH}_2)_6\text{N}_4$  (curve 3) in  $1 \text{ mol L}^{-1}$  NaOH +  $1.0 \text{ mmol L}^{-1}$  *p*-nitrophenol (scanning rate  $0.02 \text{ V s}^{-1}$ )

11, in a whole, the Ag/NiO samples with 5 % Ag content prepared each method all show the higher electrocatalytic activity for *p*-nitrophenol reduction than that with NiO, and much higher than the that with a bare GCE. The enhanced catalytic activity can be attributed to addition of Ag nanoparticles to NiO materials, for Ag nanoparticles have



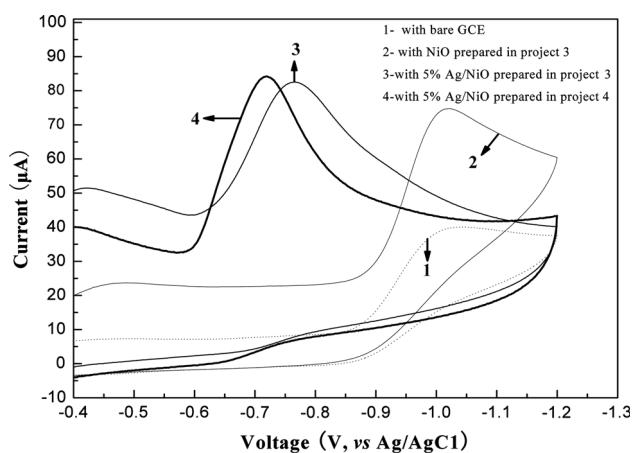


**Fig. 11** Cyclic voltammograms of a bare GCE (curve 1) and a GCE modified with NiO (curve 2) and Ag/NiO with 5 % Ag content (curve 3) prepared in method 3 and Ag/NiO with 5 % Ag content (curve 4) prepared in method 4 in  $1 \text{ mol L}^{-1}$  NaOH +  $1.0 \text{ mmol L}^{-1}$  *p*-nitrophenol (scanning rate  $0.02 \text{ V s}^{-1}$ )

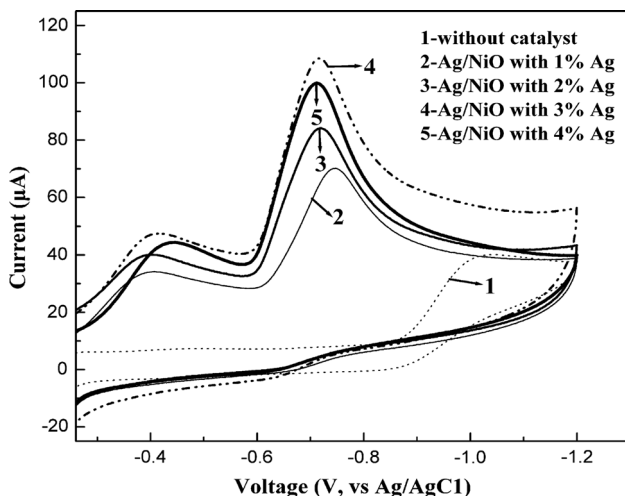


**Fig. 12** Cyclic voltammograms of a bare GCE (curve 1) and a GCE modified with Ag/NiO with different Ag contents prepared in method 4 in  $1 \text{ mol L}^{-1}$  NaOH +  $1.0 \text{ mmol L}^{-1}$  *p*-nitrophenol (scanning rate  $0.02 \text{ V s}^{-1}$ )

efficient electron transfer function and higher catalytic activity [31]. Because the peak potentials have an obvious decrease using the Ag/NiO samples, a great deal of energy can be saved as the GCE modified with the Ag/NiO samples shall be applied industrially.

To examine the effect of Ag amount on the electrocatalytic property of catalyst for *p*-nitrophenol reduction in a base solution, the GCE modified with Ag/NiO with 1, 2, 3 and 4 % Ag contents prepared in method 4 were used, respectively. The results are shown in Fig. 12. According to Fig. 12, by increasing Ag content from 1 to 4 %, all the peak potentials decreased over 0.28 V and the

corresponding peak currents increased 1.7 times bigger than that with a bare GCE. Furthermore, the peak current increases first (Ag content from 1 to 3 %) then decreases (Ag content from 3 to 4 %). The Ag/NiO sample with 3 % Ag shows the highest activity according to Figs. 11 and 12. The main reason may be due to the severe agglomeration of Ag atoms with a higher Ag content and decrease of Ag atoms in surface of Ag/NiO catalyst, leading to decrease of electrocatalytic activity.

## 4 Conclusion

Ag/NiO composite nanosheets and empty microspheres were synthesized successfully via the facile and easily controlled hydrothermal and solvothermal procedures by using four methods. The Ag nanoparticles in the nanosheets and empty microspheres have fine dispersity. The Ag/NiO composites modified on a GCE exhibited enhanced electrocatalytic activity by comparing to a bare GCE, and *p*-nitrophenol could be reduced with the larger currents at the lower potentials on the GCE modified with Ag/NiO composites prepared in each method.

**Open Access** This article is distributed under the terms of the Creative Commons Attribution License which permits any use, distribution, and reproduction in any medium, provided the original author(s) and the source are credited.

## References

- Zhang S, Zhao X, Niu H, Shi Y, Cai Y, Jiang G (2009) Superparamagnetic  $\text{Fe}_3\text{O}_4$  nanoparticles as catalysts for the catalytic oxidation of phenolic and aniline compounds. *J Hazard Mater* 167:560–566
- Kalubarme RS, Cho MS, Yun KS, Kim TS, Park CJ (2011) Catalytic characteristics of  $\text{MnO}_2$  nanostructures for the  $\text{O}_2$  reduction process. *Nanotechnology* 22:395402
- Zhou K, Wang R, Xu B, Li Y (2006) Synthesis, characterization and catalytic properties of  $\text{CuO}$  nanocrystals with various shapes. *Nanotechnology* 17:3939
- Wang CA, Li S, An L (2013) Hierarchically porous  $\text{Co}_3\text{O}_4$  hollow spheres with tunable pore structure and enhanced catalytic activity. *Chem Commun* 49:7427–7429
- Li X, Li W, Ma H, Chen J (2007) Electrochemical lithium intercalation/deintercalation of single-crystalline  $\text{V}_2\text{O}_5$  nanowires. *J Electrochem Soc* 154:A39–A42
- Sankar KV, Kalpana D, Selvan RK (2012) Electrochemical properties of microwave-assisted reflux-synthesized  $\text{Mn}_3\text{O}_4$  nanoparticles in different electrolytes for supercapacitor applications. *J Appl Electrochem* 42:463–470
- Deng J, Ma J, Mei L, Tang Y, Chen Y, Lv T, Xu Z, Wang T (2013) Porous  $\alpha\text{-Fe}_2\text{O}_3$  nanosphere-based  $\text{H}_2\text{S}$  sensor with fast response, high selectivity and enhanced sensitivity. *J Mater Chem A* 1:12400–12403
- Wang L, Kang Y, Liu X, Zhang S, Huang W, Wang S (2012) ZnO nanorod gas sensor for ethanol detection. *Sensor Actuat B Chem* 162:237–243

9. Tudisco C, Cambria MT, Bertani F, Sinatra F, Fantechi E, Innocenti C, Sangregorio C, Dalcanele E, Condorelli GG (2013) Functionalization of PEGylated  $\text{Fe}_3\text{O}_4$  magnetic nanoparticles with tetraphosphonate cavities for biomedical application. *Nanoscale* 5:11438–11446
10. Yin ZF, Wu L, Yang HG, Su YH (2013) Recent progress in biomedical applications of titanium dioxide. *Phys Chem Chem Phys* 15:4844–4858
11. Liu H, Wang G, Liu J, Qiao S, Ahn H (2011) Highly ordered mesoporous NiO anode material for lithium ion batteries with an excellent electrochemical performance. *J Mater Chem* 21:3046–3052
12. Liu J, Shi J, Yan X, Zhai X, Tao Z, Guo Q, Liu L (2012) Preparation and electrochemical properties of hollow nickel oxide fibers. *Int J Electrochem Sci* 7:2214–2220
13. Wang D, Xu R, Wang X, Li Y (2006) NiO nanorings and their unexpected catalytic property for CO oxidation. *Nanotechnology* 17:979
14. Zhou D, Yan A, Wu Y, Wu T (2013) A facile synthetic route to flower-like NiO and its catalytic properties. *Indian J Chem* 52A:51–56
15. Zhao B, Ke XK, Bao JH, Wang CL, Dong L, Chen YW, Chen HL (2009) Synthesis of flower-like NiO and effects of morphology on its catalytic properties. *J Phys Chem C* 113:14440–14447
16. Inamdar AI, Kim Y, Pawar SM, Kim JH, Im H, Kim H (2011) Chemically grown, porous, nickel oxide thin-film for electrochemical supercapacitors. *J Power Source* 196:2393–2397
17. Dar FI, Moonoswamy KR, Es-Souni M (2013) Morphology and property control of NiO nanostructures for supercapacitor applications. *Nanoscale Res Lett* 8:363
18. Wang HT, Mishra DK, Chen P, Ting JM (2014) *p*-Type dye-sensitized solar cell based on nickel oxide photocathode with or without Li doping. *J Alloys Compd* 584:142–147
19. Proenca MP, Sousa CT, Pereira AM, Tavares PB, Ventura J, Vazquez M, Araujo JP (2011) Size and surface effects on the magnetic properties of NiO nanoparticles. *Phys Chem Chem Phys* 13:9561–9567
20. Mironova-Ulmane N, Kuzmin A, Grabis J, Sildos I, Voronin VI, Berger IF, Kazantsev VA (2011) Structural and magnetic properties of nickel oxide nanopowders. *Solid State Phenom* 168–169:341–344
21. Zhang X, Gu A, Wang G, Huang Y, Ji H, Fang B (2011) Porous Cu–NiO modified glass carbon electrode enhanced nonenzymatic glucose electrochemical sensor. *Analyst* 136:5175–5180
22. Xiong QQ, Tu JP, Xia XH, Zhao XY, Gu CD, Wang XL (2013) A three-dimensional hierarchical  $\text{Fe}_2\text{O}_3$ @NiO core/shell nanorod array on carbon cloth: a new class of anode for high-performance lithium-ion batteries. *Nanoscale* 5:7906–7912
23. Zhang S, Li J, Wen T, Xu J, Wang X (2013) Magnetic  $\text{Fe}_3\text{O}_4$ @NiO hierarchical structures: preparation and their excellent As(V) and Cr(VI) removal capabilities. *RSC Adv* 3:2754–2764
24. Zhang YX, Kuang M, Wang JJ (2014) Mesoporous CuO–NiO micropolyhedrons: facile synthesis, morphological evolution and pseudocapacitive performance. *CrystEngComm* 16:492–498
25. Liu J, Jiang J, Bosman M, Fan HJ (2012) Three-dimensional tubular arrays of  $\text{MnO}_2$ –NiO nanoflakes with high areal pseudocapacitance. *J Mater Chem* 22:2419–2426
26. Wu JB, Li ZG, Huang XH, Lin Y (2013) Porous  $\text{Co}_3\text{O}_4$ /NiO core/shell nanowire array with enhanced catalytic activity for methanol electro-oxidation. *J Power Source* 224:1–5
27. Mattei G, Mazzoldi P, Post ML, Buso D, Guglielmi M, Martucci A (2007) Cookie-like Au/NiO nanoparticles with optical gas-sensing properties. *Adv Mater* 19(4):561–564
28. Kim SS, Park KW, Yum JH, Sung YE (2006) Pt–NiO nanophase electrodes for dye-sensitized solar cells. *Sol Energy Mater Sol Cells* 90:283–290
29. Wang Y, Cui X, Deng Y, Shi F (2014) Catalytic hydrogenation of aromatic rings catalyzed by Pd/NiO. *RSC Adv* 4:2729–2732
30. Husin H, Su WN, Pan CJ, Liu JY, Rick J, Yang SC, Chuang WT, Sheu HS, Hwang BJ (2013) Pd/NiO core/shell nanoparticles on  $\text{La}_0.02\text{Na}_0.98\text{TaO}_3$  catalyst for hydrogen evolution from water and aqueous methanol solution. *Int J Hydrogen Energy* 38:13529–13540
31. Wu H, Lin D, Zhang R, Pan W (2007) Facile synthesis and assembly of Ag/NiO nanofibers with high electrical conductivity. *Chem Mater* 19:1895–1897
32. Teng F, Xu T, Zheng Y, Liang S, Gochoo B, Gu X, Zong R, Yao W, Zhu Y (2008) Formation of hollow NiO single crystals and Ag/NiO flowers. *Mater Res Bull* 43:3562–3569
33. Chen YC, Zheng FC, Min YL, Wang T, Zhang YG, Wang YX, Chen YC (2012) Facile procedure to synthesize highly crystalline Ag/NiO nanocomposite microspheres and their photocatalytic activity. *J Mater Sci Mater Electron* 23:1592–1598
34. Ding Y, Wang Y, Su L, Zhang H, Lei Y (2010) Preparation and characterization of NiO–Ag nanofibers, NiO nanofibers, and porous Ag: towards the development of a highly sensitive and selective non-enzymatic glucose sensor. *J Mater Chem* 20:9918–9926
35. Liu J, Du S, Wei L, Liu H, Tian Y, Chen Y (2006) Template-free synthesis of NiO hollow microspheres covered with nanoflakes. *Mater Lett* 60:3601–3604
36. Lv J, Lai F, Lin L, Lin Y, Huang Z, Chen R (2007) Thermal stability of Ag films in air prepared by thermal evaporation. *Appl Surf Sci* 253:7036–7040
37. Zhang YG, Wang ST, Qian YT, Zhang ZD (2006) Complexing-reagent assisted synthesis of hollow CuO microspheres. *Solid State Sci* 8:462–466